# Three-Dimensional Spectroscopy of Vibrational Energy Relaxation in Liquid Methanol

**Lawrence K. Iwaki† and Dana D. Dlott***

*Department of Chemistry, University of Illinois at Urbana-Champaign, Box 01-6 CLSL, 600 South Mathews Avenue, Urbana, Illinois 61801*

*Received: June 21, 2000; In Final Form: August 3, 2000*

Vibrational energy relaxation (VER) of neat methanol at ambient temperature is studied with a three-dimensional vibrational spectroscopy technique. The first two dimensions are represented by a time series of incoherent anti-Stokes Raman spectra at a given mid-IR pump frequency. The third dimension involves changing the mid-IR pump frequency within the manifold of CH and OH stretching transitions $\nu$(CH) and $\nu$(OH). Each 2D representation shows the VER dynamics occurring as a result of pumping a specific vibrational transition. The decay of the pumped transition into first-generation daughters, and the subsequent decay into second-, and even third-generation daughters can be monitored. The third dimension shows how VER depends on the nature of the pumped transition. Additional information about the buildup of excitation in the bath of lower-energy collective excitations (phonons) is obtained by monitoring the heating of $CCl_4$ spectators in methanol−$CCl_4$ mixtures. Three distinct stages are seen in VER of $\nu$(CH). The pumped $\nu$(CH) creates two quanta of bending vibrations $\delta$(CH) or $\delta$(OH) (0−1 ps), the $\delta$(CH) vibrations preferentially create CO stretch $\nu$(CO), and the $\delta$(OH) create methyl rock $\rho(CH_3)$ (2−5 ps), and then $\rho(CH_3)$ and $\nu$(CO) decay into phonons (5−15 ps). Three stages are also seen in $\nu$(OH) VER except that the first stage involves exciting every other vibration to some extent. About 10% of $\nu$(OH) decay occurs in four stages, where the first stage is $\nu$(OH) → $\nu$(CH). The IR−Raman 3D technique is compared to other multidimensional vibrational spectroscopies. This 3D method is presently the most powerful technique for studying VER in condensed phases. It is sensitive to overtone and combination transitions buried under more intense fundamental absorption spectra. In addition it is sensitive to very weak cascaded anharmonic couplings responsible for the excitation of successive generations of daughter vibrations.

## 1. Introduction

Virtually all chemical phenomena in polyatomic liquids and solutions involve vibrational energy relaxation (VER).[1,2] VER in condensed phases is an elementary process that remains poorly understood to this day. The reasons for this lack of understanding are twofold. Calculations are problematic.[3,4] Experimentally extensive use has been made of pump−probe methods to measure the decay out of a specific higher wavenumber (say >1500 $cm^{-1}$) vibrations, but finding where the vibrational energy has gone has only been accomplished in a few cases.[5]

More than 20 years ago, Laubereau and Kaiser developed a powerful experimental technique which monitors the decay of a laser-pumped vibration (the parent) and the growth and subsequent decay of lower-frequency daughter vibrations.[6] This ultrafast infrared−Raman (IR−Raman) technique uses resonant vibrational pumping by a tunable mid-IR pulse and incoherent anti-Stokes Raman probing.[6] However, only recently have advances in laser technology allowed this technique to be used to its fullest potential, to monitor energy flow through all Raman-active vibrations, including the lower frequency states, of a polyatomic liquid or solution.[7−9]

In this paper, we report our studies of VER in liquid (neat) methanol at ambient temperature using the IR−Raman technique. Methanol (along with water) is a model system for understanding the effects of hydrogen bonding on VER, such as the dependence of VER on pump frequency within the very broad (∼700 $cm^{-1}$) OH stretching band. In a recent letter,[10] we studied vibrational energy redistribution within the C−H stretching $\nu$(CH) and O−H stretching $\nu$(OH) transitions of methanol. In this paper, we shall concentrate on determining the mechanisms of VER through direct observation of the daughters of $\nu$(CH) and $\nu$(OH) decay, and by a recently introduced technique where the build up of the collective lower-energy excitations of the bath (phonons) is detected by a $CCl_4$ spectator.[9,11,12]

Recently there has been a good deal of interest in multidimensional vibrational spectroscopy.[13] Much of our past work with the IR−Raman technique has examined VER with the pump $\omega_{IR}$ tuned to only one vibrational transition,[12] giving a time series of anti-Stokes spectra probing a wide wavenumber range (typically 800−4000 $cm^{-1}$). This time and frequency data is a 2D representation of a particular vibrational cooling (VC) process. In the present work we introduce the additional dimension of tuning the pump pulse through the mid-IR absorption, leading to a 3D vibrational spectroscopy which provides information about correlations between vibrations,[13,14] vibrational lifetimes, spectral diffusion, and anharmonic interactions[15] that couple the parents to first-, second-, and higher-generation daughters. Obtaining a complete 3D surface is extremely time-consuming and difficult, so at the present time we have measured only part of the 3D surface for methanol. Nevertheless the present results indicate a great deal of

* Author to whom correspondence should be addressed. E-mail: d-dlott@scs.uiuc.edu.

† Present address: National Institute of Standards and Technology, Gaithersburg, MD 20899-8441.

10.1021/jp002246w CCC: $19.00 
Published on Web 09/16/2000

additional information can be obtained using 3D vibrational spectroscopy.

Previous IR−Raman studies of polyatomic liquids from our laboratory and from other laboratories have been reviewed elsewhere.[6,12,16,17] As a background note, we should mention the extensive studies of ethanol ultrafast vibrational dynamics, first by the Kaiser group[18−20] and later by the Laubereau group[21−25] and others.[26−29] We chose methanol rather than ethanol for our studies because it is simpler—no possibility of energy transfer among methyl and methylene vibrations.[25] Early studies of neat ethanol[18−20,25,27] and methanol[19] were directed toward measuring C−H stretch decay and understanding the mechanism in the context of Fermi resonances with the lower-energy bending vibrations. Heilweil et al.[26] used one-color mid-IR pump probe to measure $\nu$(OH) lifetimes of ethanol and methanol monomers in $CCl_4$. Recent attention has been directed to ethanol oligomers in $CCl_4$. These hydrogen-bonded oligomers are interesting because $\nu$(OH) pumping temporarily breaks up the oligomer via vibrational predissociation.[21,22,29] One-color or two-color mid-IR pump−probe spectroscopy of ethanol oligomers has been used to measure the VER lifetime of $\nu$(OH) and $\nu$(CH),[25,27,28] orientational relaxation,[28,29] spectral diffusion,[24] and vibrational predissociation[30] following $\nu$(OH) pumping.[21,22,25,29] The two-color mid-IR techniques are complementary to the IR−Raman method. The IR−Raman method opens up a new window to VER due to its ability to probe the dynamics of the lower-frequency daughter vibrations, so the present work is focused on this issue, which has not been studied in detail previously.

In the rest of this paper, we briefly review the vibrational spectroscopy of methanol. Next we discuss aspects of the IR−Raman technique needed to understand our results, and to understand the present 3D technique. Then we present results on VER of methanol with pump pulses in the $\nu$(CH) and $\nu$(OH) regions. We also present vibrational cooling data obtained by monitoring vibrational heating of a $CCl_4$ spectator in methanol−$CCl_4$ solutions. With both types of results in mind, we then discuss what has been learned about VER in methanol and present a comprehensive picture of its VER dynamics. Finally, we compare the present technique to other multidimensional vibrational techniques and discuss the advantages of adding the third dimension.

## 2. Spectroscopy of Methanol

Figure 1 shows IR and Raman spectra of methanol. Each transition is labeled by its assignment from ref 31. There are twelve normal modes of methanol: three CH stretches and three CH bends, one OH stretch and one OH bend, two methyl rocking motions, one CO stretch, and an OH torsion. The dotted curves in the IR are representative of the spectra of the mid-IR pump pulses. In the ~3000 $cm^{-1}$ CH stretch region there are two higher-frequency $\nu_a$(CH) and one lower-frequency $\nu_s$(CH) transitions. The broad line width of the $\nu$(OH) transition is due to the simultaneous coexistence of a wide range of hydrogen-bonding environments.[32,33] Nonassociated methanol has a characteristic much sharper $\nu$(OH) transition near 3700 $cm^{-1}$[22] In neat methanol, the higher-frequency $\nu$(OH) region is associated with sites of weaker hydrogen bonding and the lower-frequency region with sites of stronger hydrogen bonding.[32,33]

The bending vibrations, $\delta_s$(CH), $\delta$(OH) and a pair of $\delta_a$(CH), the pair of methyl rock vibrations $\rho(CH_3)$, and the CO stretch $\nu$(CO) are found in the 950−1700 $cm^{-1}$ range. The OH torsion $\delta$(OH···O) is seen in the IR in the 500−800 $cm^{-1}$ range but is essentially invisible in the Raman. To deal with spectral overlap among these transitions, we used a computer program (Microcal Origin) to fit the static anti-Stokes spectrum, obtained with a high signal-to-noise ratio, by a sum of Voigt line shapes. The fitted center frequencies, which agreed well with literature values,[31] were $\delta_a$(CH) 1541 $cm^{-1}$, $\delta_s$(CH) 1466 $cm^{-1}$, $\delta$(OH) 1381 $cm^{-1}$, $\rho(CH_3)$ 1117 $cm^{-1}$, and $\nu$(CO) 1034 $cm^{-1}$. The components at 1541 and 1117 $cm^{-1}$ represent pairs of nearly degenerate $\delta_a$(CH) or $\rho(CH_3)$ transitions, which cannot be individually resolved. The fit to the static spectrum is essentially perfect. We assign no physical significance to the Voigt parameters, but use this fitting method solely to determine the instantaneous amplitude of each transition in the anti-Stokes transients. An example of a computer-generated fit to an anti-Stokes transient is shown in Figure 2. In fitting these transients, which have worse signal-to-noise ratios than the static spectrum, only the amplitude of each Voigt component is varied.

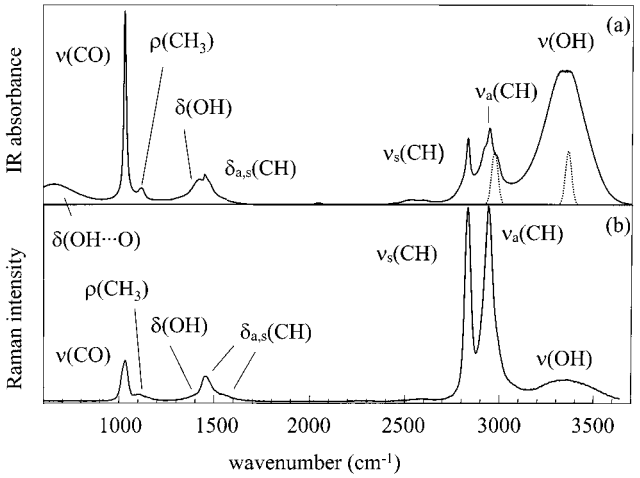


**Figure 1.** IR and Raman spectra of methanol, obtained with instrumental resolution better than the natural line widths. The assignments are from ref 31 The dotted curves under the $\nu$(CH) and $\nu$(OH) transitions are characteristic of the spectra of the mid-IR pump pulses.

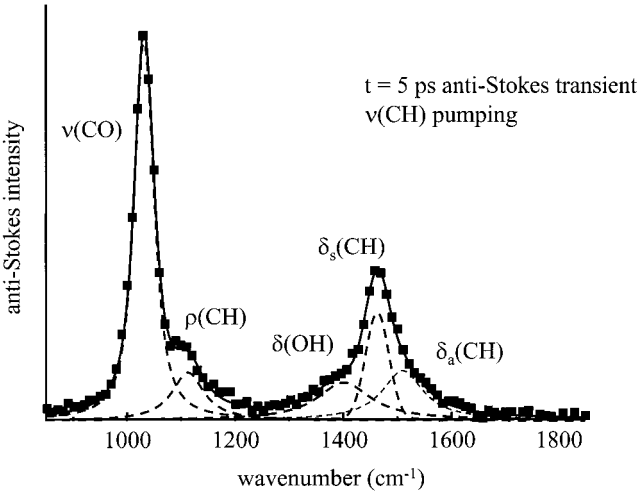


**Figure 2.** An anti-Stokes transient (delay = 5 ps, $\nu$(CH) pumping, thermal background subtracted) for vibrations in the lower frequency region. The smooth curve is a fit to the sum of five Voigt line shape functions representing the five transitions indicated in the figure. The dashed curves are the individual Voigt components whose amplitudes are varied to fit all the transient data.

## 3. IR−Raman Technique

The IR−Raman technique has been discussed in several reviews.[6,12,16,17] The mid-IR pump pulse $\omega_{IR}$ and 532 nm Raman

probe pulse $\omega_L$ used here have spectral widths of 35 and 25 $cm^{-1}$, respectively, and durations $\tau_p \sim 0.8$ ps.[34] The experiments in ambient liquids are approximately in the semi-impulsive limit[13,14,35] where

$$T_2 \sim \tau_p \leq T_1 \quad (1)$$

except in the case of $\nu$(OH) pumping, where $T_2 \ll \tau_p$. In eq 1, $T_2$ is the usual time constant for vibrational dephasing and $T_1$ the time constant for VER.[6]

**A. Pumping $\nu$(CH) and $\nu$(OH) Fundamentals**. There is no possibility of pumping $\nu$(OH) overtones ($v = 2$ or higher) because the $\nu$(OH) anharmonicity[28] is about 250 $cm^{-1}$. The $\nu$(CH) anharmonicity is much smaller, probably about 20 $cm^{-1}$ as measured for ethanol,[25] but the incident pump fluence of $\sim$0.15 J/$cm^2$ is about one-tenth of the saturation fluence for the CH stretch transition, $\sim$1.5 J/$cm^2$.[10] Therefore, $\nu$(OH) and $\nu$(CH) overtone excitation by the pump pulses is, at most, a few percent.

**B. Bulk Temperature Jump**. The ambient temperature anti-Stokes spectrum is subtracted from the transients in all displayed data as described previously.[8,36] The nonequilibrium population generated by the pump pulse eventually ($\sim$20 ps) comes to a new quasi-equilibrium at a temperature somewhat above ambient. At longer delay times, the probe pulse sees an average over the rather complicated spatial profile of the temperature jump.[17] The magnitude of the spatially averaged temperature jump is typically $\Delta T = 10-30$ K, depending on the pump frequency. At the new quasi-equilibrium, the vibrational populations reach new steady-state levels that depend on the magnitude of $\Delta T$ and the vibrational frequency[8,36] (e.g., see Figures 4 and 10−13). The temperature jump ultimately decays via thermal conduction on the $<100$ $\mu$s time scale, which is shorter than the 1 ms separation between pump pulses.

**C. Probing with Incoherent Anti-Stokes Emissio**n. For an instantaneous pump pulse arriving at time $t = 0$, the change in the anti-Stokes intensity of transition $i$, with frequency $\omega_i$, the "anti-Stokes transient" is[7]

$$\Delta I_i^{AS}(t) = const \Delta n_i(t) g_i \sigma_{Ri} (\omega_L + \omega_i)^4 \quad (2)$$

where the constant depends on the experimental set up, $\Delta n_i(t)$ is the instantaneous induced change in vibrational population, $g_i$ is the degeneracy, and $\sigma_{Ri}$ is the Raman cross-section. Equation 2 shows that the anti-Stokes transient's intensity is proportional to the population change during VER. It is possible to probe both the parent vibration and its daughters, but in a neat liquid it is not possible to tell whether the daughters are on the same molecule or on adjacent molecules.

**D. Observing Overtone or Combination Excitations**. Since $\nu$(OH) and $\nu$(CH) fundamentals are more than twice the energy of some other vibrations, mid-IR pumping could result in the excitation of first overtones $2\nu_i$ or combinations $\nu_i + \nu_j$. When the anharmonic shift is $\leq$30 $cm^{-1}$, which is often the case, we cannot resolve it very well. Since the anti-Stokes Raman cross-section is largest for single-quantum transitions, first overtones $2\nu_i$ are observed via the $2\nu_i \rightarrow \nu_i$ transition which appears as excitation of the fundamental with twice the amplitude.[7] Combinations are seen as simultaneous excitation of both $\nu_i$ and $\nu_j$.[7] Sometimes we observe the following VER process:[9]

$$\nu_i \rightarrow 2\nu_j \rightarrow \nu_j \rightarrow \text{ground} \quad (3)$$

In this case, we first see a buildup of $\nu_j$, followed by a nonexponential decay where the first part corresponds to $2\nu_j \rightarrow \nu_j$ and the second part to $\nu_j \rightarrow$ ground.

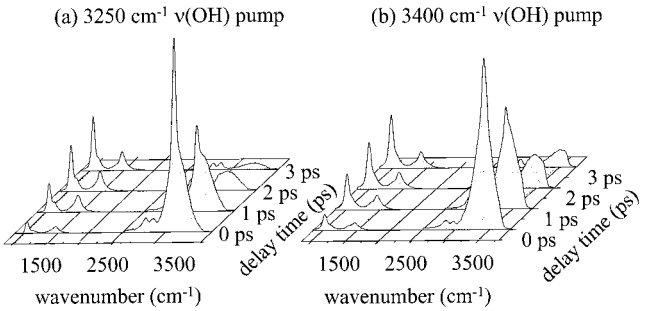


**Figure 3.** Representative data for methanol pumped at 3250 and 3400 $cm^{-1}$ in the $\nu$(OH) region. An artifact due to nonlinear elastic light scattering is seen as the sharp feature on top of the $\nu$(OH) spectrum at shorter delay times. The artifact is seen at the same anti-Stokes wavenumber as the pump pulse.

**E. Artifacts.** Coherent artifacts in IR−Raman experiments[5,19,37] and 3D mid-IR experiments[38] are often observed near $t = 0$. Artifacts are generated by elastic or inelastic nonlinear light scattering.[37,39,40] The most intense artifacts are caused by *elastic* nonlinear light scattering that appears at the sum frequency $\omega_L + \omega_{IR}$. In liquids, sum-frequency generation is forbidden in the dipole approximation but it is allowed by quadrupole or higher-order terms.[41] The elastic artifact appears at the same anti-Stokes wavenumber as the parent vibration pumped by the laser.[37] For example, Figure 3 shows methanol data where $\omega_{IR}$ is either 3250 or 3400 $cm^{-1}$. The elastic artifact is the relatively narrow feature at 3250 or 3400 $cm^{-1}$ anti-Stokes Raman shift (optical frequencies $\omega_{IR} + \omega_L$) whose intensity peaks near $t = 0$. The artifact's temporal and spectral properties can be characterized using a thin (50 $\mu$m) nonlinear crystal such as KTP ($KTiOPO_4$) as the sample.[37] The artifact can easily be subtracted from the data, since it simply rides on top of the incoherent anti-Stokes signal.

*Inelastic* nonlinear light scattering, which is a general case of hyper-Raman scattering, would appear at $\omega_L + \omega_{IR} - \omega_i$. Inelastic scattering is expected to be smaller than elastic scattering by two or more orders of magnitude,[39] which appears to be the case in our methanol experiments. For example, the most prominent inelastic signal would likely originate from the strongly Raman-active $\nu$(CO) transition ($\omega_i = 1034$ $cm^{-1}$). Its inelastic artifact would appear at either 2215 or 2366 $cm^{-1}$ for 3250 or 3400 $cm^{-1}$ pumping. Nothing is seen in this region in Figure 3; thus inelastic artifacts appear to be insignificant. We should, however, be concerned about the possibility of inelastic artifacts when monitoring a transition $\omega_i$ at about one-half the frequency of the parent $\omega_{IR}$ (e.g., CH stretch and CH bend). In that case the inelastic artifact would appear at $\omega_L + \omega_{IR}/2$, which would be coincident with anti-Stokes transient from $\omega_i$. The test for inelastic artifacts in this case is to slightly tune $\omega_{IR}$. The inelastic signal will tune along with $\omega_{IR}$, whereas the $\omega_i$ anti-Stokes signal will not.

**F. Interactions and Anti-Stokes Probing.** The most significant clues to the nature of the interactions between daughters and parents are found in the time dependence. The mid-IR pulse pumps an initial state whose character is primarily $\nu$(CH) or $\nu$(OH) fundamental. For "pure" $\nu$(CH) or $\nu$(OH) pumping, the parent population will rise instantaneously (i.e., on the $\sim$1 ps time scale of the apparatus time response) and fall on the time scale of VER. First-generation daughters are identified by a rise time that matches the parent fall time. Second-generation

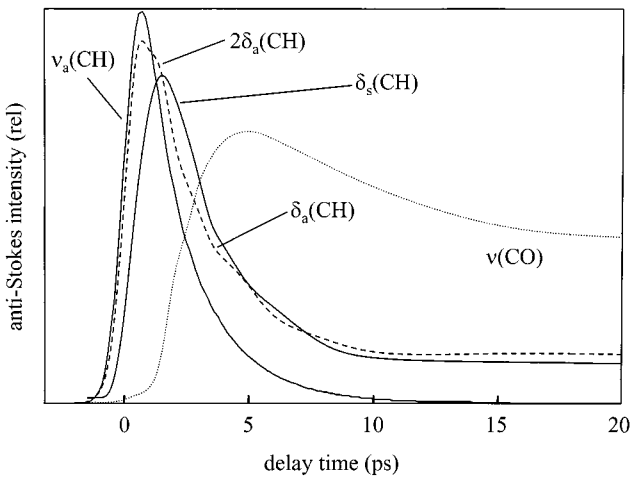


**Figure 4.** Representative anti-Stokes transients (smooth fitted curves only) seen with $\nu_a$(CH) pumping in methanol. The coupling of each vibration to the parent $\nu_a$(CH) can be understood from the build-up time. $\delta_a$(CH) rises instantaneously, indicating coherent coupling between $\nu_a$(CH) and $2\delta_a$(CH). The delayed rise of $\delta_s$(CH) indicates it is a first-generation daughter. The even slower rise of $\nu$(CO) indicates it is a second-generation daughter.

daughters are identified by a rise time that matches the first-generation fall time, and so on.

However, the initial state may in addition to the fundamental involve correlated lower-frequency states. These vibrational correlations are often the result of resonance between the fundamental and some combination or overtone.[13,14] One might view this as a combination or overtone that is buried under the more intense fundamental absorption. In this case the parent state is an admixture of higher- and lower-frequency excitations which would be expected to rise and decay in a concerted fashion. This situation is illustrated in Figure 4 for the case of $\nu_a$(CH) pumping at $\omega_{IR} = 2980$ cm$^{-1}$. This pump pulse is in the region of Fermi resonance between $\nu_a$(CH) and $2\delta_a$(CH). For clarity in Figure 4, we display only the smooth curves that fit the individual data points of the anti-Stokes transients (the data points themselves, normalized by their respective Raman cross-sections, are shown in Figure 11).

The parent $\nu_a$(CH) signal rises instantaneously, and then decays nonexponentially as a result of a competition between VER and equilibration with $\nu_s$(CH). The instantaneous rise of $\delta_a$(CH) in Figure 4 indicates a strong correlation with the pumped $\nu_a$(CH) state. As expressed by eq 3 above, the $\delta_a$(CH) transient is at first primarily the overtone $2\delta_a$(CH) and later the fundamental $\delta_a$(CH). The instantaneous rise of $2\delta_a$(CH) excitation indicates that energy exchange with $\nu_a$(CH) is faster than ~0.2 ps. A lower limit to $T_2$ for $\nu$(CH) can be estimated from the line widths of $\nu$(CH) transitions in methanol (30−40 cm$^{-1}$ from Figure 1b), to be $T_2 > 0.2$ ps. Energy exchange on time scales comparable to or faster than $T_2$ indicates the existence of *coherent vibrational coupling* between $\nu_a$(CH) and $2\delta_a$(CH). The $\delta_s$(CH) transient in Figure 4 rises on the 1−2 ps time scale of $\nu_a$(CH) decay, indicating that $\delta_s$(CH) is a first-generation daughter. The $\nu$(CO) transient rises on the 3−4 ps time scale of $\delta_a$(CH) and $\delta_s$(CH) decay, indicating it is a second-generation daughter.

The coupling between the parent and the first-generation $\delta_s$(CH) and $\delta_a$(CH) daughters might be either cubic $\langle V^{(3)}\rangle$, or quartic $\langle V^{(4)}\rangle$ anharmonic coupling.[15] An example of cubic coupling is

$$\nu_a(\text{CH})\ 2980\ \text{cm}^{-1} \rightarrow \delta_a(\text{CH})\ 1580\ \text{cm}^{-1} + \delta(\text{OH})\ 1400\ \text{cm}^{-1} \quad (4)$$

where energy conservation is possible due to the finite widths of the bending transitions. An example of quartic anharmonic coupling is

$$\nu_a(\text{CH})\ 2980\ \text{cm}^{-1} \rightarrow \delta_s(\text{CH})\ 1466\ \text{cm}^{-1} + \delta(\text{OH})\ 1381\ \text{cm}^{-1} + \text{phonon}\ 133\ \text{cm}^{-1} \quad (5)$$

where the daughter vibrations are near the peaks of the vibrational density of states, and energy is conserved by emitting one phonon. The cubic or quartic matrix elements in eqs 4 and 5 are quite small. In contrast to the usual anharmonicity of a particular mode, for instance the ~20 cm$^{-1}$ anharmonicity for $\nu$(CH) or $\delta$(CH) in methanol, these are *mixed mode anharmonicities*. Mixed mode anharmonicities are usually small because they couple different vibrations and/or phonons.[15] For instance, experiments[42,43] and calculations[42,44] on crystalline naphthalene give an average value for the cubic anharmonicity for two vibrations and one phonon of $\langle V^{(3)}\rangle \sim 0.05$ cm$^{-1}$. The rise times of first-generation daughter anti-Stokes transients provide estimates of anharmonic couplings that are possibly more than 2 orders of magnitude smaller than the vibrational line widths.

The $\nu$(CO) excitation is a second-generation daughter created from $\delta$(CH) in a two-step process such as

$$\nu_a(\text{CH}) \rightarrow \delta(\text{CH}) \rightarrow \nu(\text{CO}) \quad (6)$$

This scheme is actually a representation of several more complicated processes. One example might be

$$\nu_a(\text{CH}) \rightarrow \delta_s(\text{CH}) + \delta_a(\text{CH}) \rightarrow \nu(\text{CO}) + \text{phonon} + \delta_a(\text{CH}) \rightarrow \cdots \quad (7)$$

The interaction between the parent $\nu_a$(CH) and the second-generation daughter $\nu$(CO) in eq 7 is formally some higher-order (i.e., sixth or seventh order) anharmonic coupling. This higher-order coupling actually consists of *cascaded* cubic or quartic interactions, which might be expressed as $\langle V^{(3)}\rangle\langle V'^{(3)}\rangle$, $\langle V^{(4)}\rangle\langle V'^{(3)}\rangle$, etc. These cascaded interactions are obviously very much smaller than the vibrational line width, and might be as small as $10^{-3}$−$10^{-4}$ cm$^{-1}$.

**G. 3D Vibrational Spectroscopy**. Our 3D data will be presented in the form of a time series of 2D plots with $x$ and $y$ wavenumber axes. The signal along the diagonal at $t = 0$ is due to elastic artifacts plus the parent population. The artifact's intensity along the diagonal is a sum-frequency spectrum where $\omega_{IR}$ is scanned, $\omega_L$ is fixed, and the detector is kept at $\omega_L + \omega_{IR}$. The population contribution along the diagonal at $t = 0$ is approximately proportional to the products of the mid-IR and Raman cross-sections. Off-diagonal signals at $t = 0$ should in principle be due to vibrations that are strongly correlated with the pumped vibration. In practice, $t = 0$ signals also have a contribution from first-generation daughters that are produced during the ~1 ps pump pulses. For $t > 0$, off-diagonal signals are associated with daughters generated by VER, which reveal weaker correlations due to mixed-mode anharmonic coupling or cascaded mixed-mode anharmonic coupling.

## 4. Experimental Section

The IR−Raman system, consisting of a ~1 ps Ti:sapphire laser and a two-color $KTiOPO_4$ optical parametric amplifier,

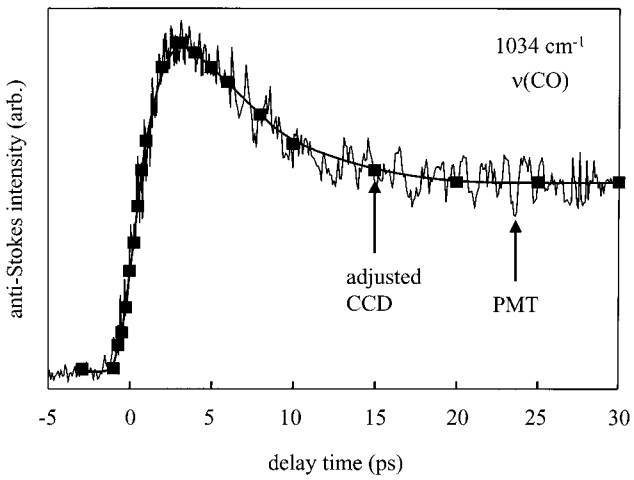


**Figure 5.** Schematic of normalization procedure to remove effects of long-term laser drift. The anti-Stokes signal from $\nu$(CO) is isolated with a narrow-bandwidth spectrometer and photomultiplier (PMT). The signal is averaged over many sweeps of the delay line (solid curve). A smooth curve is fit to the PMT data. The time-dependent $\nu$(CO) signal amplitude from the charge-coupled array detector (CCD) is corrected using the smooth curve.

has been described previously.[5,34] The pump pulses (2.7−3.5 $\mu$m, ∼50 $\mu$J, ∼0.8 ps, 35 cm$^{-1}$ fwhm, 200 $\mu$m diameter) and probe pulses (0.532 $\mu$m, 5 $\mu$J, ∼0.8 ps, 25 cm$^{-1}$ fwhm, 150 $\mu$m diameter) were focused on a flowing jet of reagent grade methanol (Aldrich). The $CCl_4$ experiments used a mixture of methanol with 25% $CCl_4$ (Aldrich). Anti-Stokes emission was detected with a spectrograph and charge-coupled array detector (CCD), or with a monochromator and a photomultiplier tube (PMT). Data were acquired at five pump wavenumbers, 2870, 2970, 3033, 3250 and 3400 cm$^{-1}$.

The multichannel CCD detector is preferred for detecting the anti-Stokes signal, since it captures the entire spectrum simultaneously. However, obtaining a series of CCD spectra over a range of delay times takes many hours, during which the laser intensity and alignment may drift. The effects of these drift factors can be corrected by using a PMT scan. With the PMT, we average many (typically 10−20) scans of the delay line, each scan lasting only a few minutes. This averaged scan eliminates effects of long-term drift. For a normalizing PMT scan, the most intense, best-resolved transition should be used, which in methanol is $\nu$(CO). Figure 2 shows that with an ∼50 cm$^{-1}$ detection window near 1000 cm$^{-1}$, only $\nu$(CO) is detected. A $\nu$(CO) PMT scan is shown in Figure 5, along with a smooth curve fit to the data. Each CCD spectrum was corrected for drift by multiplying it by a factor (generally in the 0.8 to 1.2 range), that makes the $\nu$(CO) time dependence from the CCD match the time dependence from the PMT.

## 5. Results

**A. CH and OH Stretch Pumping**. Figure 6 shows some representative data (artifacts removed) for $\nu$(CH) and $\nu$(OH) pumping. To understand how VER depends on the parent, we need to characterize energy redistribution in the $\nu$(CH) and $\nu$(OH) manifolds. In previous work we studied equilibration between $\nu_s$(CH) and $\nu_a$(CH).[10] When pumping at lower frequency, about one-fourth of $\nu_s$(CH) is transferred to $\nu_a$(CH) before VER. When pumping at higher frequency, about one-third of $\nu_a$(CH) is transferred to $\nu_s$(CH) before VER. Thus with lower frequency $\nu_s$(CH) pumping or higher frequency $\nu_a$(CH) pumping, the VER we see originates predominantly but not entirely from the pumped $\nu_a$(CH) or $\nu_s$(CH) state. Figure 6 shows that little $\nu$(OH) is produced with $\nu$(CH) pumping. In fact, detectable amounts of $\nu$(OH) are produced only when $\nu$(CH) is pumped in the higher-frequency region, and we believe it is produced not by $\nu$(CH) → $\nu$(OH) energy transfer but by direct laser absorption into the red tail of the $\nu$(OH) absorption.[10]

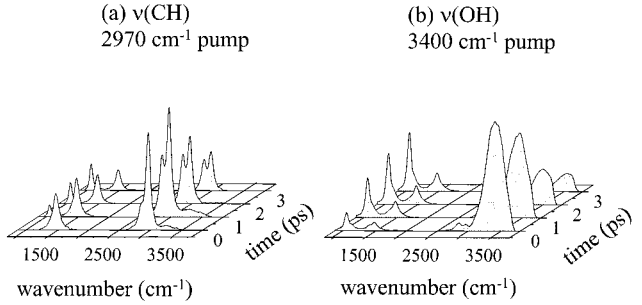


**Figure 6.** Methanol data with artifact removed for $\nu$(CH) and $\nu$(OH) pumping.

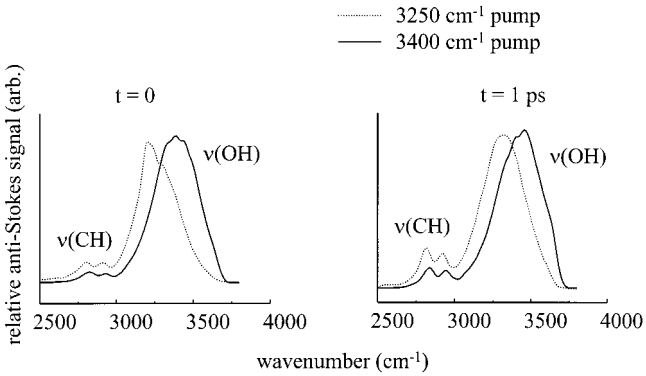


**Figure 7.** Spectral diffusion in $\nu$(OH) smears out the initial distribution produced by pumping at higher or lower wavenumber. During the 0−1 ps range when most $\nu$(OH) relaxation occurs, 3250 cm$^{-1}$ pumping produces a somewhat red-shifted population and 3400 cm$^{-1}$ pumping produces a somewhat blue-shifted population.

There is a small amount of $\nu$(OH) → $\nu$(CH) energy transfer (∼10%, see Figure 6b). A more serious concern is spectral diffusion in $\nu$(OH). The $\nu$(OH) transition is inhomogeneously broadened[12,24] and the ∼35 cm$^{-1}$ pump pulse produces a somewhat narrowed excitation distribution that broadens due to spectral diffusion. Spectral diffusion might be caused by equilibrium structural fluctuations,[24] structural fluctuations triggered by $\nu$(OH) pumping,[37,45] or $\nu$(OH) excitation hopping to different local environments.[37,46,47] The observed VER thus involves excitations at the pump frequency plus any other $\nu$(OH) that becomes excited by spectral diffusion during the 1−2 ps $\nu$(OH) lifetime.[37] Figure 7 compares $\nu$(OH) excitations in the 0−1 ps time range with lower wavenumber 3250 cm$^{-1}$ and higher wavenumber 3400 cm$^{-1}$ pumping. These two pump wavenumbers do produce somewhat different $\nu$(OH) populations.

**B. $CCl_4$ Experiments**. Using $CCl_4$ as a spectator to probe the buildup of bath excitation during VER was discussed previously.[11,12,17] The $CCl_4$ is heated primarily by phonons produced by methanol vibrational cooling. We pumped both $\nu$(CH) and $\nu$(OH) of methanol (the pump pulses are not absorbed by $CCl_4$) and probed three low-wavenumber $CCl_4$ Raman transitions (314, 459, and 790 cm$^{-1}$). $CCl_4$ did not noticeably affect methanol VER except that $\Delta T$ was slightly smaller in solution. Even with 25% $CCl_4$ low-molecular-weight alcohols remain highly associated.[48] The $CCl_4$ anti-Stokes transients are

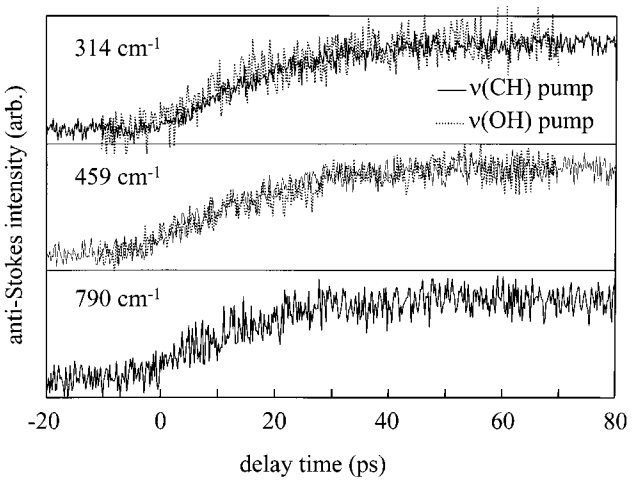


**Figure 8.** Rise of vibrational excitation from three $CCl_4$ transitions in methanol−$CCl_4$ solution (75% methanol, 25% $CCl_4$). Solid curves are for $\nu$(CH) pumping, dotted curves for $\nu$(OH) pumping. The buildup is complete within 20 ps, indicating there is no significant VER in methanol after 20 ps. There is no evidence for a fast burst of energy at short times, suggesting the initial steps in $\nu$(CH) and $\nu$(OH) relaxation are primarily intramolecular.

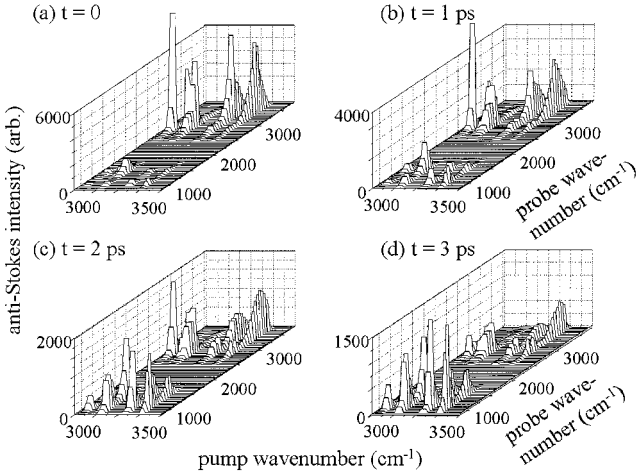


**Figure 9.** Three-dimensional methanol data. The data were obtained at five different pump wavenumbers in the 2800−3500 $cm^{-1}$ range. The data from each pump wavenumber are plotted as a strip ~50 $cm^{-1}$ wide to indicate the instrumental spectral resolution. Empty regions between these five strips do not indicate a lack of signal, but rather the lack of data in these regions.

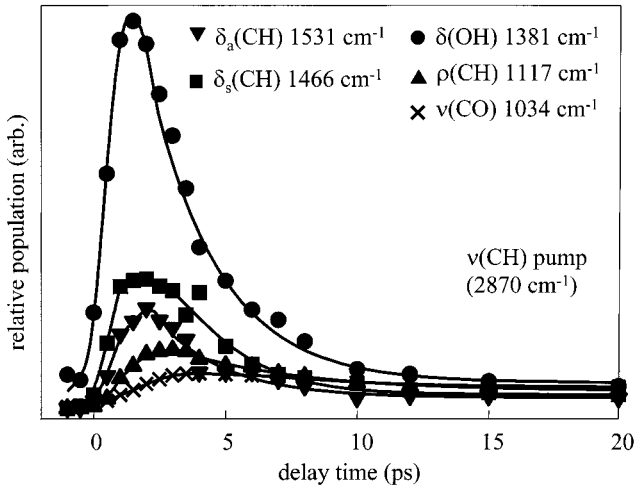


**Figure 10.** Time dependence of the relative populations of methanol vibrations with $\nu$(CH) pumping at 2870 $cm^{-1}$.

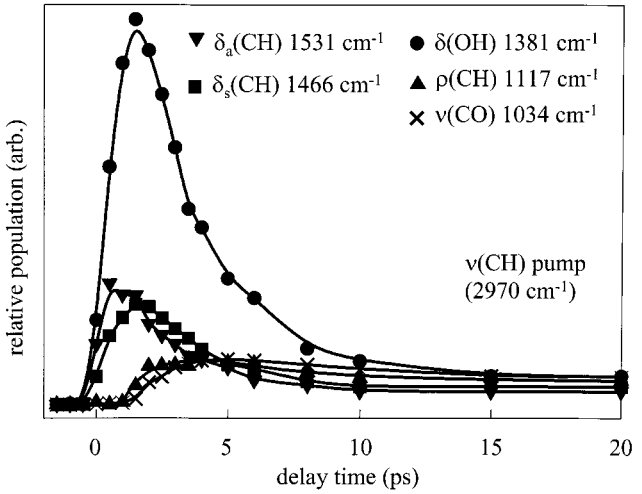


**Figure 11.** Time dependence of the relative populations of methanol vibrations with $\nu$(CH) pumping at 2970 $cm^{-1}$.

shown in Figure 8. The signal-to-noise ratio is poor due to a large thermal background for these lower-frequency $CCl_4$ vibrations. Within experimental error, the anti-Stokes transients for the three probed $CCl_4$ vibrations with either $\nu$(OH) or $\nu$-(CH) pumping were essentially identical, with the buildup of $CCl_4$ excitation complete within about 20 ps. That demonstrates unambiguously that there is no vibrational energy stored in methanol after ~20 ps. This is important because Raman probing does not see the $\delta$(OH···O) torsion and we need to determine whether stored vibrational energy is hiding in this state. The $CCl_4$ buildup in the first 2 ps is no more than 10−15%, suggesting that the relaxation of $\nu$(CH) and $\nu$(OH) is primarily intramolecular. We cannot definitively rule out the alternative possibility of slow (~20 ps) response of $CCl_4$ to bath heating by methanol, but in the past we have seen much faster (<3 ps) vibrational heating of $CCl_4$ by acetonitrile.[9]

**C. 3D Representation**. A 3D representation of the methanol data is shown in Figure 9. Artifacts were not removed. For each pump wavenumber, we plot a 50 $cm^{-1}$ wide strip that approximately represents the apparatus spectral resolution (35 $cm^{-1}$ pump and 25 $cm^{-1}$ probe). Two features are worth noting: (1) at the present time we have data only at five pump wavelengths, so vacant strips along the abscissa *do not indicate the absence of signal, but rather the absence of data*; (2) the 2D plots are rectangular because the wavenumber range probed via anti-Stokes scattering is much larger than the range of pump tuning.

In Figure 9a ($t = 0$), the largest signals are the coherent artifacts on the diagonal. The off-diagonal signals provide information about vibrational correlations.[13,14] However keep in mind that the off-diagonal signals are *intensities*. The off-diagonal populations are the intensities divided by the Raman cross-sections, which vary quite a bit. The smaller cross-sections tend to de-emphasize $\delta$(OH), $\delta_a$(CH), and $\rho(CH_3)$ at the expense of the more intense $\delta_s$(CH) and $\nu$(CO).

**D. Methanol VER**. In Figures 10−13, we have plotted the time-dependent *relative populations* of the daughter vibrations excited by different wavenumber pump pulses—2 different locations within the $\nu$(CH) manifold and two different locations within the $\nu$(OH) manifold. In these figures, the time-dependent amplitudes of the bending and stretching transitions, determined with the spectrum-fitting procedure discussed in conjunction

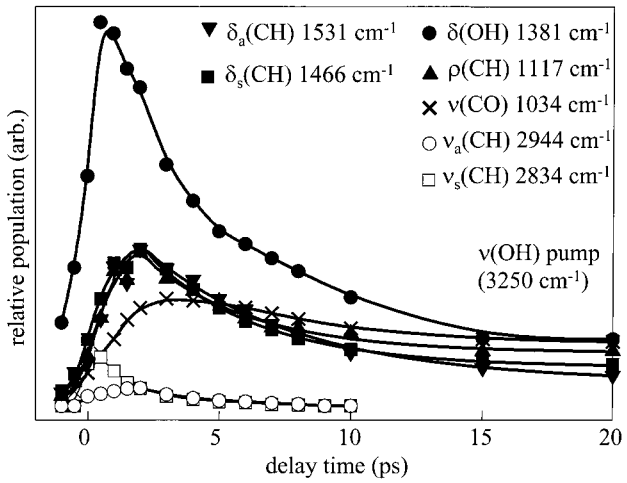


**Figure 12.** Time dependence of the relative populations of methanol vibrations with $\nu$(OH) pumping at 3250 cm$^{-1}$.

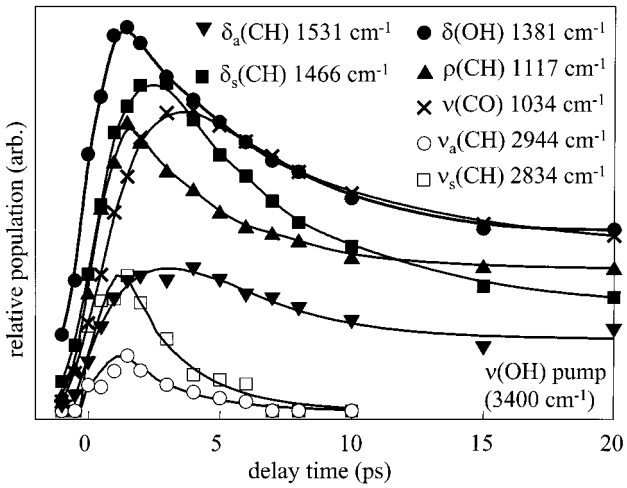


**Figure 13.** Time dependence of the relative populations of methanol vibrations with $\nu$(OH) pumping at 3400 cm$^{-1}$.

with Figure 2, are normalized by Raman cross-sections from steady-state spectra.

*i. 2870 cm$^{-1}$ Pumping.* The pumped $\nu_s$(CH) excitations are below the region of Fermi resonance with $2\delta_a$(CH). Three stages of VER are seen in Figure 10. In the first stage, $\nu$(CH) decay occurring in the 0−1 ps range generates the three bending vibrations $\delta$(OH), $\delta_s$(CH),and $\delta_a$(CH). The $\delta$(OH) population is about three times larger than the other bending vibrations. In the second stage the three bending vibrations generate $\rho(CH_3)$ and $\nu$(CO) in the 2−5 ps range. The $\rho(CH_3)$ population is about twice the $\nu$(CO) population. The delayed buildup of $\rho(CH_3)$ and $\nu$(CO) is a bit difficult to see in Figure 10, but easy to see in Figure 4 where the $\nu$(CO) transient is expanded. In the third stage, $\rho(CH_3)$ and $\nu$(CO) decay into bath excitations in the 5−15 ps time range. These bath excitations are not observed directly, but their buildup is indirectly detected by $CCl_4$ heating (Figure 8).

*ii. 2970 cm$^{-1}$ Pumping.* The pumped $\nu_a$(CH) excitations are in the Fermi resonance region. The overall three-stage VER process is similar to what was seen with 2870 cm$^{-1}$ pumping, with two differences. First, as discussed in conjunction with Figure 4, pumping in the Fermi resonance region leads to the instantaneous appearance of $2\delta_a$(CH) excitation along with the pumped $\nu_a$(CH). Thus in the first stage of VER, there is relatively more $\delta_a$(CH) than with 2870 cm$^{-1}$ pumping. In the second stage of VER, there is relatively less $\rho(CH_3)$ and more $\nu$(CO) than with 2870 cm$^{-1}$ pumping.

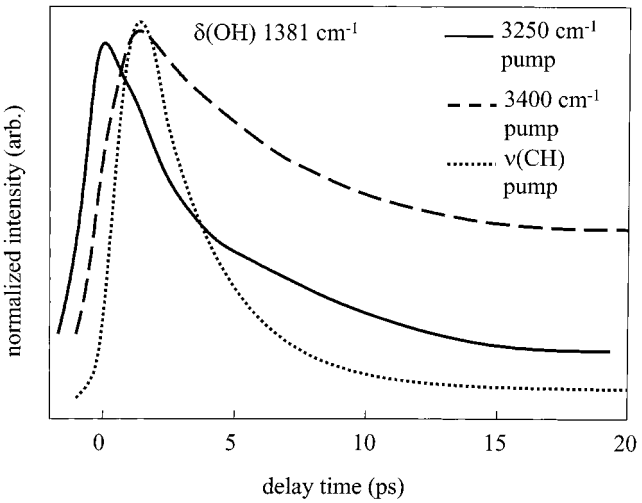


**Figure 14.** Comparison of $\delta$(OH) transients (all normalized to the same height) with different pump wavenumbers. At 3250 cm$^{-1}$ in the lower wavenumber part of the $\nu$(OH) transition, an instantaneous rise of $\delta$-(OH) is observed indicating the mid-IR pulse is pumping a buried transition that contains substantial $\delta$(OH) character.

*iii. 3250 cm$^{-1}$ Pumping.* This pump wavenumber produces VER from a red-shifted $\nu$(OH) population, as shown in Figure 7. The population dynamics are shown in Figure 12. $\nu$(OH) relaxation is qualitatively different from $\nu$(CH) relaxation. $\nu$-(OH) decay immediately produces excitations *in all observed lower-frequency methanol vibrations*.

An interesting and totally unexpected result is seen in Figure 12—the instantaneous appearance of $\delta$(OH) excitations. This effect is more easily seen in Figure 14, where we compare expanded and normalized $\delta$(OH) anti-Stokes signals at different pump wavenumbers. The $\delta$(OH) rise follows the decay of pumped $\nu$(CH) or $\nu$(OH) except for 3250 cm$^{-1}$ pumping, where $\delta$(OH) appearance is instantaneous. We cannot conclude that we are producing a coherently coupled $\nu$(OH) and $\delta$(OH) state, as in the case of $\nu$(CH) pumping in the Fermi resonance region, because the pulse is ∼1 ps whereas $T_2$ for $\nu$(OH) very much shorter—perhaps the inverse of the ∼300 cm$^{-1}$ $\nu$(OH) line width seen in Figure 7 or ∼30 fs.

*iv. 3400 cm$^{-1}$ Pumping.* This pump wavenumber produces a somewhat blue-shifted $\nu$(OH) population (see Figure 7). Figure 13 shows that $\nu$(OH) relaxation generates all the lower-frequency vibrations. Unlike 3250 cm$^{-1}$ pumping, there is no instantaneous appearance of $\delta$(OH). In comparison to 3250 cm$^{-1}$ pumping, where $\delta$(OH) dominates, 3400 cm$^{-1}$ pumping produces roughly equal amounts of $\delta$(OH), $\delta_s$(CH), $\rho(CH_3)$, and $\nu$(OH). There is much less $\delta_a$(CH) and more $\nu_s$(CH).

**E. Vibrational Predissociation**. It is well-known that $\nu$(OH) pumping of gas-phase methanol clusters leads to cluster fragmentation via vibrational predissociation.[49] Efficient (∼70%) vibrational predissociation was first observed in condensed phase ethanol oligomers in $CCl_4$ by Laubereau et al.[21,25] The Laubereau experiments monitored the appearance of the vibrational ground state of the nonassociated $\nu$(OH) transition. Anti-Stokes probing, which sees only excited states, is not suitable for this task. Stokes probing of nonassociated $\nu$(OH) is possible, provided the signal is above the background of the associated methanol. In a limited number of Stokes probing experiments, we found no evidence for a nonassociated $\nu$(OH) after 3250 cm$^{-1}$ pumping.

## 6. Discussion

Two topics will be discussed in this section: (1) VER in methanol, and (2) the present 3D IR−Raman technique and comparison to other multidimensional techniques.

**A. VER in Methanol**. It is worthwhile mentioning that isolated gas-phase methanol will not undergo VER when either $\nu$(CH) and $\nu$(OH) *fundamentals* are pumped. The density of states is simply too small to permit efficient intramolecular vibrational relaxation (IVR).[50] All the VER phenomena seen here are a consequence of intermolecular interactions in the condensed-phase environment.

We do not observe the appearance of the nonassociated methanol transition created by vibrational predissociation following $\nu$(OH) pumping, even though predissociation has been seen in many studies of ethanol oligomers.[21,22,29] Efficient predissociation is inconsistent with the $CCl_4$ data in Figure 8, because predissociation would release a large burst (1000−2000 $cm^{-1}$) of energy[49] into the bath on the 0−2 ps time scale of $\nu$(OH) decay, which is not seen. We stress that our experiments are performed on neat alcohol rather than alcohol oligomers. In oligomers, vibrational predissociation of molecules at the end of open oligomer chains[21,22,29] produces easily detectable monomeric $\nu$(OH). In neat methanol, every methanol molecule is part of an extensive hydrogen-bonded network and essentially all molecules have multiple hydrogen bonds.[33] Even if a single hydrogen bond were broken, the result might not possess a transition that was spectroscopically distinguishable from other associated species. In addition the total concentration of nonassociated alcohol would likely never be very great, because any broken hydrogen bonds would reform much faster than in oligomers. In 1.5 M ethanol solutions, hydrogen-bond reformation occurs on the 15 ps time scale.[21,22,29] By extrapolation, in neat (25 M) methanol diffusion-controlled hydrogen-bond reformation would occur on the 1 ps time scale. It might be worthwhile to view our $\nu$(OH) pumping experiments in the following way. $\nu$(OH) pumping of neat methanol might in some environments lead to a fast hydrogen-bond disruption and reformation process that changes the local environment. In fact, a sudden change in local environment triggered by $\nu$(OH) pumping might be the cause of the spectral diffusion seen in Figure 7.

*i. CH Stretch Relaxation*. The $\nu$(CH) relaxation proceeds in three stages. In the first stage the bending vibrations $\delta$(OH), $\delta_s$(CH), and $\delta_a$(CH) are produced (1−2 ps). In the second stage, these bending vibrations generate $\rho(CH_3)$ and $\nu$(CO) (2−5 ps). In the third stage, $\rho(CH_3)$ and $\nu$(CO) decay into the bath (5−15 ps). The bending fundamentals are about one-half of the energy of the $\nu$(CH) fundamental. Thus $\nu$(CH) decay in the first 1−2 ps could produce either two bending excitations or a single bend and a large burst (∼1500 $cm^{-1}$) of energy in the bath. This large burst would be expected to cause a fast jump in the $CCl_4$ data and in the buildup of the lower-frequency $\nu$(CO) and $\rho(CH_3)$ vibrations via multiphonon up-pumping, which is not seen. Because we cannot readily distinguish between $v = 1$ and $v = 2$ bends, there are two possibilities for $\nu$(CH) relaxation. The first possibility is that bending vibrations are generated in matched pairs:

$$\nu(\mathrm{CH}) \rightarrow 2\delta(\mathrm{OH})\ (62\%, 63\%) \tag{8a}$$

$$\nu(\mathrm{CH}) \rightarrow 2\delta_a(\mathrm{CH})\ (16\%, 18\%) \tag{8b}$$

$$\nu(\mathrm{CH}) \rightarrow 2\delta_s(\mathrm{CH})\ (21\%, 18\%) \tag{8c}$$

In equations 8, $2\delta$ might represent a bend overtone on one molecule or a pair of fundamentals on two adjacent molecules. The former possibility is judged more likely because intramolecular anharmonic coupling is generally larger than intermolecular coupling. The first and second percentage efficiencies in parentheses refer to 2870 and 2970 $cm^{-1}$ pumping, respectively. A second possibility is that mixed pairs are generated. In that case VER producing $\delta$(OH) as the dominant product would occur via three channels of roughly equal efficiency:

$$\nu(\mathrm{CH}) \rightarrow 2\delta(\mathrm{OH}) \tag{9a}$$

$$\nu(\mathrm{CH}) \rightarrow \delta_a(\mathrm{CH}) + \delta(\mathrm{OH}) \tag{9b}$$

$$\nu(\mathrm{CH}) \rightarrow \delta_s(\mathrm{CH}) + \delta(\mathrm{OH}) \tag{9c}$$

*ii. CH and OH Bend Relaxation*. Relaxation of the first-generation bending vibrations generates $\rho(CH_3)$ and $\nu$(CO). Due to the energy gap for bend relaxation (∼1500 $cm^{-1}$ → ∼1000 $cm^{-1}$), this process would dissipate about one-third of the bend energy into the bath in the 2−4 ps time range. Notice that is exactly what is seen in the $CCl_4$ data in Figure 8. In the mid-IR spectrum of methanol, a broad peak extending from 500 to 800 $cm^{-1}$ has been assigned to OH torsional motion, indicated by $\delta$(OH···O) in Figure 1. It is likely that the bend relaxation generates either $\rho(CH_3)$ or $\nu$(CO) plus one torsion. It is possible to correlate the different bends with $\rho(CH_3)$ or $\nu$(CO) by looking at the pump wavenumber dependence. The big difference between 2870 and 2970 $cm^{-1}$ pumping is the extra $\delta_a$(CH) at 2970 $cm^{-1}$, and the big difference between 3250 and 3400 $cm^{-1}$ pumping is the extra $\delta$(OH) at 3250 $cm^{-1}$. Comparing Figures 10 and 11, when there is extra $\delta_a$(CH), there is proportionately more $\nu$(CO) and less $\rho(CH_3)$. Comparing Figures 12 and 13, when there is extra $\delta$(OH), there is proportionately more $\rho(CH_3)$ and less $\nu$(CO) (Because $\rho(CH_3)$ and $\nu$(CO) are generated in two stages with $\nu$(OH) pumping we look at the 2−5 ps time range of the second stage of VER). These observations seem to indicate that $\delta$(CH) has a preference for generating $\nu$(CO) while $\delta$(OH) has a preference for generating $\rho(CH_3)$:

$$\delta_a(\mathrm{CH}),\ \delta_s(\mathrm{CH}) \rightarrow \nu(\mathrm{CO}) + \text{torsion} \tag{10}$$

and

$$\delta(\mathrm{OH}) \rightarrow \rho(\mathrm{CH_3}) + \text{torsion} \tag{11}$$

*iii. CH Rock and CO Stretch Relaxation*. There are no lower energy intramolecular vibrations. These excitations relax directly to the bath. The most likely route is generation of a pair of torsional excitations on the 5−15 ps time scale, although the possibility of emitting a larger number of phonons cannot be discounted.

*iv. OH Stretch Relaxation*. There are a myriad of possibilities, so we begin by considering the simplest: generation of vibrations only, or generation of vibrations plus only a single torsion. For vibrations only, energy conservation allows for several combinations of three quanta of $\rho(CH_3)$ or $\nu$(CO). With 3400 $cm^{-1}$ relaxation, energy conservation is also possible using one quantum of $\delta$(OH) and two of the others. Thus we would expect the first generation to consist almost entirely of $\rho(CH_3)$ and $\nu$(CO), which is inconsistent with Figures 12 and 13. For generation of a single torsion in the 500−800 $cm^{-1}$ range, higher-frequency $\nu$(OH) relaxation can occur via

$$\nu(\mathrm{OH}) \rightarrow \text{any bend} + \text{either } \nu(\mathrm{CO}) \text{ or } \rho(\mathrm{CH_3}) + \text{torsion} \tag{12}$$

$$\nu(\mathrm{OH}) \rightarrow \text{any two bends} + \text{torsion} \quad (13)$$

or

$$\nu(\mathrm{OH}) \rightarrow \nu(\mathrm{CH}) + \text{torsion} \quad (14)$$

Assuming the possibility that the processes described in eqs 12 and 13 are about equally likely would give the observed first-generation abundances of bend, rock, and CO stretch.

For lower-frequency $\nu$(OH) relaxation, eqs 13,14 are not possible, so eq 12 would be expected to dominate. The domination of eq 12 implies that the first generation bend population would be about the same as the $\rho(CH_3)$ and $\nu$(CO) populations, and that is what is observed in Figure 12 if we ignore the excess $\delta$(OH) produced by direct laser pumping.

For $\nu$(OH) $\rightarrow$ $\nu$(CH), if we take the lowest wavenumber torsion to be $\sim$500 cm$^{-1}$ and the lowest wavenumber $\nu$(CH) to be $\nu_s$(CH) $\approx$ 2834 cm$^{-1}$, eq 14 is possible only for $\nu$(OH) excitations above $\sim$3350 cm$^{-1}$. In comparing Figures 12 and 13, we see a substantial increase in $\nu_s$(CH) with 3400 cm$^{-1}$ pumping, along with a dramatic drop in $\delta_a$(CH). That indicates when energy conservation allows it, eq 14 is more efficient than eq 13, presumably because eq 14 involves cubic anharmonic coupling whereas eq 13 involves quartic coupling.

*v. Vibrational Energy Flow in Methanol.* In this section we describe in broad terms what 3D spectroscopy has taught us about VER in methanol. For $\nu$(CH) pumping, VER occurs in three distinct stages, which may be summarized as follows:

$\nu$(CH) $\rightarrow$

2 bending vibrations $\delta_a$(CH), $\delta_s$(CH), $\delta$(OH) (0$-$1 ps) (1st)

$\delta_a$(CH) or $\delta_s$(CH) $\rightarrow$ $\nu$(CO) plus torsion (2$-$5 ps) (2nd)

$\delta$(OH) $\rightarrow$ $\rho(CH_3)$ plus torsion (2$-$5 ps) (2nd)

$\rho(CH_3)$ or $\nu$(CH) $\rightarrow$ 2 torsions (5$-$15 ps) (3rd)

For $\nu$(OH) pumping, the first generation includes *every other methanol vibration*—$\nu$(CH), the bending vibrations, and $\rho(CH_3)$ and $\nu$(OH). About 10% of the VER occurs in four stages, $\nu$(OH) $\rightarrow$ $\nu$(CH) + torsion followed by the three stages of $\nu$(CH) relaxation given above. The three-stage $\nu$(OH) relaxation that accounts for the other 90% of VER may be summarized as follows:

$\nu$(OH) $\rightarrow$

bend + torsion + either $\rho(CH_3)$ or $\nu$(CO) (0$-$1 ps) (1st)

$\nu$(OH) $\rightarrow$ 2 bends + torsion (0$-$1 ps) (1st)

$\rho(CH_3)$ or $\nu$(CO) $\rightarrow$ 2 torsions (5$-$15 ps) (2nd)

$\delta$(OH) $\rightarrow$ $\rho(CH_3)$ plus torsion (2$-$5 ps) (2nd)

$\delta_a$(CH) or $\delta_s$(CH) $\rightarrow$ $\nu$(CO) plus torsion (2$-$5 ps) (2nd)

$\rho$(CH) or $\nu$(CO) $\rightarrow$ 2 torsions (5$-$15 ps) (3rd)

In the scheme above, the second line is significant only for higher-frequency $\nu$(OH). In the third line above, $\rho(CH_3)$ and $\nu$(CO) are created in the first stage by $\nu$(OH) decay. In the last line, $\rho(CH_3)$ and $\nu$(CO) are created in the second stage by $\delta$(CH) or $\delta$(OH) decay.

*vi. Buildup of Bath Excitation.* These proposed mechanisms can be tested against the $CCl_4$ data. The primary routes from intramolecular vibrations to the bath appear to involve generating torsional excitations from 500 to 800 cm$^{-1}$. Due to the large anharmonicity associated with large-amplitude torsions, this should result in fast decay into phonons. Either the torsions themselves or the phonons could heat the $CCl_4$.

For $\nu$(CH) pump, in the first stage (0$-$1 ps) $\nu$(CH) generates two bends and no torsions. In the second stage, each of the two bends generates one lower energy vibration and one torsion. In the third stage, each of the two remaining vibrations generates two torsions. There are on average 6 torsions generated, two in the 2$-$5 ps range and four in the 5$-$15 ps range, which explains the data in Figure 8 very well. For $\nu$(OH) pump, things are only slightly different. There are on average 7 rather than 6 torsions generated, with the one additional torsion generated in the first 0$-$1 ps (the first stage). That implies a small-amplitude ($\sim$15%) fast component in the $CCl_4$ buildup for $\nu$(OH) pumping that would be absent with $\nu$(CH) pumping. However, such an effect could not be seen with the present signal-to-noise ratio.

*vii. Strongly Correlated Vibrational Transitions*. On the basis of instantaneously rising populations, we have detected strong correlations between $\boldsymbol{\delta}_a$(CH) and $\boldsymbol{\nu}_a$(CH) in the Fermi resonance region, and $\boldsymbol{\delta}$(OH) and $\boldsymbol{\nu}$(OH) in the lower wavenumber region of $\boldsymbol{\nu}$(OH) near 3250 cm$^{-1}$. Coherent coupling between a stretch and a bend overtone in the Fermi region is, of course, totally expected. However, the $\boldsymbol{\delta}$(OH) observation is unexpected and it is difficult to explain why this happens and why we do not see it with 3400 cm$^{-1}$ pumping (Figure 13). One possibility is that we are pumping a hot-band transition $2\boldsymbol{\delta}$(OH) + torsion ($\sim$500 cm$^{-1}$) near 3250 cm$^{-1}$. For 3400 cm$^{-1}$ pumping, a higher-energy torsion would be needed which would have a smaller thermal population. An intriguing possibility is that pumping in this lower-frequency region associated with stronger hydrogen bonding does lead to some fast vibrational predissociation that generates $\boldsymbol{\delta}$(OH) excitations. The instantaneous $\boldsymbol{\delta}$(OH) might be the spectroscopic signal of predissociation in neat methanol.

*viii. Solvent-Assisted IVR and IVR Threshold*. The concepts of intramolecular vibrational relaxation (IVR) and an IVR "threshold" are familiar from studies of gas-phase molecules.[51] Below the threshold, few or no final states (combinations of vibrations) can be found that conserve energy. In condensed phases, VER occurs well below the gas-phase IVR threshold due to the presence of a continuous spectrum of phonons.[15] Here we point out that purely intramolecular relaxation processes may themselves be quite different in condensed phases. In condensed phases, every vibrational state is broadened by fast energy exchange with the solvent.[52] For example, Figure 2 shows that the lower-frequency methanol vibrations have line widths of $\sim$100 cm$^{-1}$. Therefore in condensed phase IVR, energy-conserving intramolecular pathways can be found at much lower threshold energies, for example, in the IVR of $\nu$(CH) at $\sim$3000 cm$^{-1}$. Thus, we might speak of "solvent-assisted IVR" that cannot occur in the gas phase.

There is a qualitative change in the solvent-assisted IVR when the energy of the pump pulse crosses the threshold that separates $\nu$(CH) from $\nu$(OH). With $\nu$(CH) VER, some of the methanol vibrations, namely $\nu$(CO) and $\rho(CH_3)$, are not populated in the initial burst of energy relaxation. With $\nu$(OH) pumping, *all vibrations* are populated in the initial burst of energy relaxation. That is presumably because new channels (eqs 12 and 14) have opened up that allow direct energy transfer from $\nu$(OH) to $\nu$(CH), $\nu$(CO), and $\rho(CH_3)$. Thus, we might speak of a *solvent-*

*enhanced IVR threshold* in condensed-phase methanol slightly above 3000 $cm^{-1}$, where vibrational energy flows freely into every vibration in the molecule.

**B. Comparison to Other Multidimensional Techniques**. Multidimensional vibrational spectroscopy has been the subject of several recent reviews.[13,14] There are many kinds of multidimensional spectroscopies. Here we compare the 3D IR−Raman method to some well-known multidimensional techniques: time-domain 2D fifth-order Raman experiments, frequency-domain 2D doubly vibrational enhanced four-wave mixing (DOVE-FWM), and 2D and 3D experiments using ultrashort mid-IR pulses.

Multidimensional vibrational experiments can be categorized by the pump and probe process.[13,14] Some techniques use Raman excitation and probing (visible light only), mid-IR pumping and probing (mid-IR only), or a combination of mid-IR and visible. The pump process may be impulsive, quasi-continuous, or quasi-impulsive, where the latter means longer than a vibrational period but shorter than most characteristic relaxation times.[13,14] The probe process may be coherent or incoherent.

*i. Fifth-Order Raman Techniques*. Time-domain fifth-order Raman experiments with impulsive pulses are attractive because of the correspondence with well-developed magnetic resonance techniques.[13,14] There are two delay time variables $\tau_1$ and $\tau_2$, and a phase-sensitive detection scheme. The signal can be expressed in 2D as a function of $\tau_1$ and $\tau_2$, or as a function of frequency (wavenumber) axes $\omega_1$ and $\omega_2$ via Fourier transform. Available pulse sources ($\geq$20 fs) limit these measurements to the lower wavenumber (say $<$500 $cm^{-1}$) transitions. Combination bands, which appear as cross-peaks off the diagonal, reveal correlations between different transitions which might be exploited to learn about molecular structure and dynamics. In principle, homogeneous and inhomogeneous dephasing times as well as energy relaxation times can be determined from a complete set of 2D data. In practice it has proven difficult to even obtain the desired fifth-order signal against the background of cascaded third-order signals of lesser interest,[53] although the situation is improving rapidly.[54−56] To our knowledge no information about energy relaxation times has yet been obtained from this technique. Presumably this is because Raman pumping with short visible pulses does not cause much population transfer, so the population decay part of the signal is too small to be seen.

*ii. Frequency-Domain 2D Techniques*. DOVE-FWM experiments are 2D experiments that use two narrow-band quasi-continuous lasers.[57,58] The technique has been employed with two mid-IR lasers or one IR and one visible laser. The data are expressed in 2D as a function of $\omega_1$ and $\omega_2$, which are determined using spectrometers that read out the laser or signal frequency. High signal-to-noise ratio 2D signals have been obtained on several molecular liquids and solutions. Cross-peaks appear off the diagonal that represent correlated vibrational pairs (combination bands) such as $\nu_2 + \nu_4$ of acetonitrile. These DOVE techniques have been shown to be useful analytical methods that offer possible advantages such as removal of solvent background.[57,58] Although not explicitly time dependent, some information about dephasing and energy relaxation times can extracted due to an implicit time dependence in the expressions for the signal strength.

*iii. Time-Domain 2D IR*. A 2D IR technique was recently demonstrated by the Fayer laboratory,[59] using a pair of time-delayed one-color mid-IR pulses and coherent detection of the two-pulse vibrational echo signal. The data are expressed in 2D as a time series of mid-IR spectra. At zero time delay, the echo spectrum discriminates in favor of species with large cross-sections. For instance a solvent background (higher concentration, smaller mid-IR cross-section) might be removed to reveal a solute transition (lower concentration, larger mid-IR cross-section). At longer time delays, the echo spectrum discriminates in favor of species with larger cross-sections *and* slower vibrational dephasing (larger $T_2$).

*iv. Time-Domain 3D IR*. 3D IR experiments use a pair of independently tunable mid-IR pulses $\omega_1$ and $\omega_2$ in the semi-impulsive limit. The detected signal may be incoherent (pump−probe absorption recovery) or coherent (echo). The 3D signal can be expressed in two ways: 2D plots of a time series of mid-IR spectra ($\omega_2$ vs $\tau$) at different pump wavelengths $\omega_1$, or a time series of 2D plots as a function of two wavelengths ($\omega_1$ vs $\omega_2$). For example, Laubereau[22,60−63] and other authors[29,45,47,64−66] used two narrow-band picosecond or femtosecond pulses, while Hamm and Hochstrasser[67−70] used a narrow-band picosecond pulse $\omega_1$ and a broad-band femtosecond pulse monitored with a spectrograph and mid-IR array detector that simultaneously measures a range of $\omega_2$. Pump−probe has been used to study VER and spectral diffusion in the $\nu$(OH) band of isotopically substituted water solutions (HDO in $D_2O$).[45,47,61,63−66,71] Laubereau et al. used 3D pump−probe to study VER, orientational relaxation, spectral diffusion, and hydrogen bond dynamics including vibrational predissociation in ethanol oligomers and other polyatomic liquids.[22,60−63] Hochstrasser et al. studied the dynamics of amide I vibrations (1600−1700 $cm^{-1}$) of small peptides and proteins.[67−70] Pump−probe techniques were used to measure the amide VER lifetime, while stimulated echoes were used to study spectral diffusion. A combination of pump−probe and dynamic hole-burning measurements was used to provide information about the instantaneous structures of peptides.

Two-color mid-IR methods are tremendously powerful. One feature of 2-color IR experiments is worth mentioning: the probe pulse sees three effects: stimulated emission from $v = 1$ vibrations, absorption decrease from the $v = 0$ vibrational hole, and transitions to higher excited states such as $v = 1 \rightarrow 2$. The ability to see all three effects simultaneously might be viewed as a virtue or alternatively as a complication hindering data interpretation.[45]

*v. 3D IR−Raman.* The IR−Raman technique used here features semi-impulsive pumping and probing, both with reasonable spectral resolution. The probe method is strictly incoherent. Although signals are weak and interference from a variety of optical background sources is problematic,[12] there are several advantages to this method. Even though the mid-IR tuning range is limited (with our apparatus 2700−4000 $cm^{-1}$), this technique features *simultaneous probing of all lower- and higher-frequency transitions*. The incoherent signal comes only from excited states, with no contribution from the ground-state hole or transitions to higher excited states. This results in a tremendous simplification (or alternatively a significant limitation).

The 2D IR−Raman technique can be used to understand VER from a particular initial state, and for hole-burning studies of inhomogeneous broadening and spectral diffusion, especially in associated liquids such as methanol and water.[12,37] Adding the third dimension of tuning the pump shows how VER or spectral diffusion is affected by changing the initial state. For instance, we see VER is different from $\nu$(CH) or $\nu$(OH) in methanol. That is hardly unexpected. However, we also see that VER can be considerably different for different locations *within* the $\nu$(CH) and $\nu$(OH) transition. Even a change of pump wavenumber of 60 $cm^{-1}$ within the ~400 $cm^{-1}$ wide $\nu$(CH)

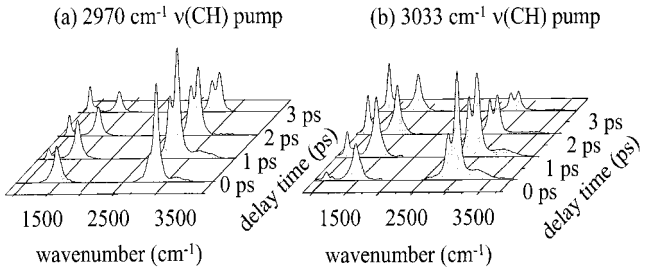


**Figure 15.** Even a small change of pump wavenumber (~60 $cm^{-1}$ change within the ~400 $cm^{-1}$ wide $\nu$(CH) manifold) can have a noticeable effect on the vibrational population distribution.

manifold can have a noticeable effect, as illustrated in Figure 15. The figure shows that tuning the pump ~60 $cm^{-1}$ to the blue, from 2970 to 3033 $cm^{-1}$, increases the abundance of $\nu$(CO), $\rho(CH_3)$, and $\nu$(OH).

The 3D technique has many other significant features. It provides an effective way of detecting vibrational correlations that are not seen by conventional methods. As the pump is tuned through the intense $\nu$(CH) and $\nu$(OH) fundamental transitions, overtone and combination bands buried under these transitions are detected via the instantaneous rise of excitation in the lower frequency states. One observed correlation was the expected coherent coupling between $\nu_a$(CH) and $2\delta_a$(CH) via Fermi resonance. A surprising new observation was a correlation between the lower frequency $\nu$(OH) states and $\delta$(OH), that does not exist with the higher frequency $\nu$(OH) states.

The IR−Raman technique reveals the existence of extremely weak but extremely interesting correlations. For example we have determined the following process occurs after 3400 $cm^{-1}$ pumping:

$$\nu(\mathrm{OH}) \rightarrow \nu_s(\mathrm{CH}) \rightarrow 2\delta(\mathrm{CH}) \rightarrow \nu(\mathrm{CO}) + \text{torsion} \quad (15)$$

This process is the result of an extremely weak interaction that might be described as a ninth-order anharmonic coupling, or better as a cascade of three third-order couplings. Somewhere under the $\nu$(OH) transition near 3400 $cm^{-1}$ is buried an incredibly weak transition involving simultaneous excitation of one quantum of $\nu$(CH), 2 quanta of $\delta$(CH), one quantum of $\nu$(CO), and one quantum of torsion. It is practically inconceivable that this correlation could be revealed using conventional IR spectroscopy to detect the absorption of the buried transition.

The 3D implementation has also proven valuable in understanding the mechanism of VER of the lower-frequency daughter vibrations. Even though instrumental limitations prevent us from directly pumping the bending fundamentals $\delta$(CH) and $\delta$(OH) in the 6.5−7.3 $\mu$m range, we have learned a great deal about their VER by tuning the pump frequency. We increase or decrease the relative populations of the different bending vibrations and then see how that affects the populations in later stages. That allowed us to determine the tendency for $\delta$(CH) to generate $\nu$(CO) and for $\delta$(OH) to generate $\rho(CH_3)$.

## 7. Conclusion

The 3D IR−Raman technique shows how VER occurs in methanol with unprecedented detail. Of particular interest is how VER changes as the pump pulse is tuned through the methanol absorption, and how measuring the dependence of VER on pump frequency helps elucidate the fundamental mechanisms of VER. The dependence on pump frequency is not entirely destroyed by fast equilibration between $\nu_s$(CH) and $\nu_a$(CH) and fast spectral diffusion in $\nu$(OH). Relatively small differences in the first stage of VER can lead to more dramatic differences in later stages. A solvent-enhanced IVR threshold has been observed. Excitation above this threshold (>3000 $cm^{-1}$) results in a fast intramolecular process not possible in isolated molecules, that redistributes the initial excitation among all other vibrations of the molecule. The surprising observation of instantaneous generation of $\delta$(OH) when pumping $\nu$(OH) at lower frequency might be an indication that some vibrational predissociation does occur in neat methanol.

**Acknowledgment.** We thank John C. Deàk for his many contributions. This material is based on work supported by the National Science Foundation under award number DMR-9714843, and by the Air Force Office of Scientific Research under contract F49620-97-1-0056. L.K.I. acknowledges support from an AASERT fellowship, DAAG55-98-1-0191, from the Army Research Office.

## References and Notes

(1) Voth, G. A.; Hochstrasser, R. M. *J. Phys. Chem.* **1996**, *100*, 13034.
(2) Stratt, R. M.; Maroncelli, M. *J. Phys. Chem.* **1996**, *100*, 12981.
(3) Egorov, S. A.; Everitt, K. F.; Skinner, J. L. *J. Phys. Chem. A* **1999**, *103*, 9494.
(4) Everitt, K. F.; Egorov, S. A.; Skinner, J. L. *Chem. Phys.* **1998**, *235*, 115.
(5) Deàk, J. C.; Iwaki, L. K.; Rhea, S. T.; Dlott, D. D. *J. Raman Spectrosc.* **2000**, *31*, 263.
(6) Laubereau, A.; Kaiser, W. *Rev. Mod. Phys.* **1978**, *50*, 607.
(7) Graener, H.; Zürl, R.; Hofmann, M. *J. Phys. Chem.* **1997**, *101*, 1745.
(8) Chen, S.; Hong, X.; Hill, J. R.; Dlott, D. D. *J. Phys. Chem.* **1995**, *99*, 4525.
(9) Deàk, J. C.; Iwaki, L. K.; Dlott, D. D. *J. Phys. Chem.* **1998**, *102*, 8193.
(10) Iwaki, L. K.; Dlott, D. D. *Chem. Phys. Lett.* **2000**, *321*, 419.
(11) Iwaki, L. K.; Deàk, J. C.; Rhea, S. T.; Dlott, D. D. *Chem. Phys. Lett.* **1999**, *303*, 176.
(12) Deàk, J. C.; Iwaki, L. K.; Dlott, D. D. *J. Phys. Chem. A* **1999**, *103*, 971.
(13) Mukamel, S. *Annu. Rev. Phys. Chem.* **2000**, in press.
(14) Mukamel, S.; Piryatinski, A.; Chernyak, V. *Acct. Chem. Res.* **1999**, *32*, 145.
(15) Kenkre, V. M.; Tokmakoff, A.; Fayer, M. D. *J. Chem. Phys.* **1994**, *101*, 10618.
(16) Seilmeier, A.; Kaiser, W. Ultrashort intramolecular and intermolecular vibrational energy transfer of polyatomic molecules in liquids. In *Ultrashort Laser Pulses and Applications*; Kaiser, W., Ed.; Springer-Verlag: Berlin, 1988; Vol. 60, p 279.
(17) Iwaki, L. K.; Deàk, J. C.; Rhea, S. T.; Dlott, D. D. Vibrational energy redistribution in polyatomic liquids: Ultrafast IR−Raman spectroscopy. In *Ultrafast Infrared and Raman Spectroscopy*; Fayer, M. D., Ed.; Marcel Dekker: New York, 2000.
(18) Laubereau, A.; Kehl, G.; Kaiser, W. *Opt. Commun.* **1974**, *11*, 74.
(19) Fendt, A.; Fischer, S. F.; Kaiser, W. *Chem. Phys.* **1981**, *57*, 55.
(20) Spanner, K.; Laubereau, A.; Kaiser, W. *Chem. Phys. Lett.* **1976**, *44*, 88.
(21) Graener, H.; Ye, T. Q.; Laubereau, A. *J. Chem. Phys.* **1989**, *91*, 1043.
(22) Graener, H.; Ye, T. Q.; Laubereau, A. *J. Chem. Phys.* **1989**, *90*, 3413.
(23) Graener, H.; Seifert, G.; Laubereau, A. *Chem. Phys. Lett.* **1990**, *172*, 435.
(24) Laenen, R.; Rauscher, C.; Laubereau, A. *J. Phys. Chem. A* **1997**, *101*, 3201.
(25) Laenen, R.; Rauscher, C.; Laubereau, A. *Chem. Phys. Lett.* **1998**, *283*, 7.
(26) Heilweil, E. J.; Casassa, M. P.; Cavanagh, R. R.; Stephenson, J. C. *J. Chem. Phys.* **1986**, *85*, 5004.
(27) Laenen, R.; Rauscher, C. *Chem. Phys. Lett.* **1997**, *274*, 63.
(28) Laenen, R.; Simeonidis, K. *Chem. Phys. Lett.* **1999**, *299*, 589.
(29) Woutersen, S.; Emmerichs, U.; Bakker, H. J. *J. Chem. Phys.* **1997**, *107*, 1483.
(30) Staib, A.; Hynes, J. T. *Chem. Phys. Lett.* **1993**, *204*, 197.
(31) Shimanouchi, T. *Tables of Molecular Vibrational Frequencies: Consolidated Volume I*; U.S. Department of Commerce, National Bureau of Standards: Washington, DC, 1972.
(32) Liddel, U.; Becker, E. D. *Spectrochem. Acta* **1957**, *10*, 70.

(33) Matsumoto, M.; Gubbins, K. E. *J. Chem. Phys.* **1990**, *93*, 1981.
(34) Deàk, J. C.; Iwaki, L. K.; Dlott, D. D. *Opt. Lett.* **1997**, *22*, 1796.
(35) Mukamel, S. *Principles of Nonlinear Optical Spectroscopy*; Oxford University Press: New York, 1995.
(36) Chen, S.; Tolbert, W. A.; Dlott, D. D. *J. Phys. Chem.* **1994**, *98*, 7759.
(37) Deàk, J. C.; Iwaki, L. K.; Dlott, D. D. *J. Phys. Chem.* **2000**, *104*, 4866.
(38) Woutersen, S.; Bakker, H. J. *J. Opt. Soc. Am. B* **2000**, *17*, 827.
(39) Terhune, R. W.; Maker, P. D.; Savage, C. M. *Phys. Rev. Lett.* **1965**, *14*, 681.
(40) Kauranen, M.; Persoons, P. *J. Chem. Phys.* **1996**, *104*, 3445.
(41) Shen, Y. R. *Surf. Sci.* **1994**, *299/300*, 551.
(42) Hill, J. R.; Dlott, D. D. *J. Chem. Phys.* **1988**, *89*, 842.
(43) Schosser, C. L.; Dlott, D. D. *J. Chem. Phys.* **1984**, *80*, 1394.
(44) Righini, R. *Chem. Phys.* **1984**, *84*, 97.
(45) Woutersen, S.; Bakker, H. J. *Phys. Rev. Lett.* **1999**, *83*, 2077.
(46) Woutersen, S. Femtosecond vibrational dynamics of hydrogen-bonded systems. Ph.D. Thesis, FOM-Institute for Atomic and Molecular Physics, 1999.
(47) Woutersen, S.; Bakker, H. J. *Nature* **1999**, *402*, 507.
(48) Coburn, W. C., Jr.; Gruwald, E. *J. Chem. Phys.* **1957**, *80*, 1318.
(49) Buck, U.; Ettischer, I. *J. Chem. Phys.* **1998**, *108*, 33.
(50) Wang, X.; Perry, D. S. *J. Chem. Phys.* **1998**, *109*, 10795.
(51) Uzer, T. *Phys. Rep.* **1991**, *199*, 73.
(52) Shelby, R. M.; Harris, C. B.; Cornelius, P. A. *J. Chem. Phys.* **1979**, *70*.
(53) Blank, D. A.; Kaufman, L. J.; Fleming, G. R. *J. Chem. Phys.* **1999**, *111*, 3105.
(54) Astinov, V.; Kubarych, K. J.; Milne, C. J.; Miller, R. J. D. *Opt. Lett.* **2000**, *25*, 853.
(55) Blank, D. A.; Kaufman, L. J.; Fleming, G. R. In press.
(56) Golonzka, O.; Demirdöven, N.; Tokmakoff, A. In press.
(57) Zhao, W.; Wright, J. C. *J. Am. Chem. Soc.* **1999**, *121*, 10994.
(58) Zhao, W.; Wright, J. C. *Phys. Rev. Lett.* **2000**, *84*, 1411.
(59) Rector, K. D.; Fayer, M. D.; Engholm, J. R.; Crosson, E.; Smith, T. I.; Schwettman, H. A. *Chem. Phys. Lett.* **1999**, *305*, 51.
(60) Graener, H.; Dohlus, R.; Laubereau, A. *Chem. Phys. Lett.* **1987**, *140*, 306.
(61) Graener, H.; Seifert, G.; Laubereau, A. *Phys. Rev. Lett.* **1991**, *66*, 2092.
(62) Laenen, R.; Rauscher, C.; Laubereau, A. *J. Phys. Chem. B* **1998**, *102*, 9304.
(63) Laenen, R.; Rauscher, C.; Laubereau, A. *Phys. Rev. Lett.* **1998**, *80*, 2622.
(64) Woutersen, S.; Emmerichs, U.; Bakker, H. J. *Science* **1997**, *278*, 658.
(65) Woutersen, S.; Emmerichs, U.; Nienhuys, H.-K.; Bakker, H. *Phys. Rev. Lett.* **1998**, *81*, 1106.
(66) Gale, G. M.; Gallot, G.; Hache, F.; Lascoux, N.; Bratos, S.; Leicknam, J.-C. *Phys. Rev. Lett.* **1999**, *82*, 1068.
(67) Hamm, P.; Lim, M.; Hochstrasser, R. M. *Biophys. J.* **1998**, *74*, A332.
(68) Hamm, P.; Lim, M.; DeGrado, W. F.; Hochstrasser, R. M. *J. Chem. Phys.* **2000**, *112*, 1907.
(69) Hamm, P.; Lim, M.; DeGrado, W. F.; Hochstrasser, R. M. *J. Phys. Chem. A* **1999**, *103*, 10049.
(70) Hamm, P.; Limm, M.; Hochstrasser, R. M. *J. Phys. Chem. B* **1998**, *102*, 6123.
(71) Nienhuys, H.-K.; Woutersen, S.; van Santen, R. A.; Bakker, H. J. *J. Chem. Phys.* **1999**, *111*, 1494.